ELSEVIER

Chemical Physics 195 (1995) 59–69

Chemical Physics

# A perturbation treatment of oscillating magnetic fields in the radical pair mechanism using the Liouville equation

J.M. Canfield [a,*], R.L. Belford [b], P.G. Debrunner [a], K. Schulten [a,b,c]

[a] *Department of Physics, University of Illinois at Urbana-Champaign, Urbana, IL 61801, USA*
[b] *Department of Chemistry, University of Illinois at Urbana-Champaign, Urbana, IL 61801, USA*
[c] *Beckman Institute, University of Illinois at Urbana-Champaign, Urbana, IL 61801, USA*

Received 10 August 1994; in final form 14 January 1995

**Abstract**

This paper describes an application of time-dependent perturbation theory to the calculation of singlet-to-triplet yields in radical pair reactions for oscillating magnetic fields. It outlines an iterative approach, based on the Liouville equation, that holds for any order of perturbation theory. It then compares this method to other methods, namely, numerical integration and the rotating frame treatment as well as methods based on the Schrödinger equation, and gives sample results.

## 1. Introduction

This work was stimulated in part by the continued interest in the magnetic sense in animals [1,2] as well as the growing concern over health effects of sub-thermal nonionizing oscillating electromagnetic fields [3,4]. One physical mechanism that has been proposed to account for biological effects of magnetic fields is the radical pair mechanism [5–11]. This mechanism has proven quite successful in explaining the effects of steady as well as microwave magnetic fields on the photosynthetic reaction center (see, for example, Refs. [12–16]).

The purpose of this paper is to further examine the effects of oscillating magnetic fields on chemical reaction yields within the radical pair mechanism. It seeks a general treatment that can apply to a combination of a steady field with multiple oscillating fields, all at different frequencies and orientations with respect to the steady field. Since this work is aimed toward biological effects of magnetic fields and, in particular, magnetic sensory mechanisms, it should be sufficient to develop a general treatment that can hold in the natural magnetic environment. This is because the natural magnetic field undergoes slight variations in magnitude and direction with time and location, and these variations can provide information on direction, location, time of day, or season to animals capable of detecting them [17]. Thus, certain animals may have evolved sensitivity to the natural magnetic environment, and effects due to man-made magnetic environments, which have not existed long on an evolutionary time-scale, are probably only incidental.

Thus, since the geomagnetic field is typically

* Corresponding author; email: canfield@rlb6000.scs.uiuc.edu.


*SSDI* 0301-0104(95)00049-6

composed of a steady field of 0.5 G and a spectrum of oscillating fields with intensities well below 0.03 G (a fluctuation due to a very large magnetic storm) [17], in order to hold in the natural magnetic environment, the general treatment is restricted in that it must be able to handle very weak steady fields but enjoys the freedom that it can use perturbation theory to treat the effects of the oscillating fields. This use of perturbation theory should also be applicable to a number of man-made magnetic environments where the steady field is much larger than the oscillating fields. Thus, a general treatment based on perturbation theory should be useful in certain health effects studies as well.

In a previous paper [18], a perturbation expansion for the effects of oscillating magnetic fields in the radical pair mechanism was presented. This expansion was based on the Schrödinger equation. The present paper discusses a similar expansion, this time in the framework of the Liouville equation. Both methods give the same results if the singlet and triplet states depopulate with equal rates ($k_S = k_T$) in the Liouville method and an exponential time dependence ($\tau$ = time constant) is assumed in the Schrödinger method. In this limit where $k_S = k_T = 1/\tau$, the spin and cage dynamics decouple (here cage dynamics includes the effects of chemical reactions and diffusion). Nevertheless, the Liouville equation allows a more general treatment that includes the effects of coupled spin and cage dynamics. This allows one to treat more thoroughly systems expressed by kinetic equations. This formalism also allows a more natural description of more complicated effects such as rotation, spin relaxation, diffusion, and multi-step reaction kinetics (state diagrams).

In addition to the increased rigor and generality of the Liouville equation approach, the perturbation method outlined below happens to yield a more reliable, compact, and efficient computer algorithm than did the Schrödinger approach. This new approach does not suffer from certain numerical problems arising in the Schrödinger approach such as occur when evaluating integrals (31) and (32) in Ref. [18] near $\omega = 0$, especially for higher orders of perturbation theory. It also does not suffer from the rapidly increasing computation times needed for the Schrödinger approach, thus allowing much higher orders to be done in a reasonable time frame.

## 2. Radical pair mechanism in the Liouville formalism

The radical pair mechanism [19–21] can be applied when two unpaired electron spins ($S_1$ and $S_2$) coexist in a cage long enough to undergo spin dynamics (variation in singlet/triplet character with time) due, for example, to their interactions with external magnetic fields $B(t)$ through the Zeeman effect, with nearby nuclear spins $I_j$ through the hyperfine coupling $a_j$, and with each other via the exchange interaction $J$. Typically such a pair is formed in a singlet state by a homolytic cleavage of a covalent bond, and one needs to determine the chance that such a pair will escape rather than recombine. Since recombination typically occurs only in the singlet state [19, p. 15], the spin dynamics and all the terms controlling it (such as the external magnetic field) are very important for determining the chance that the pair will escape. To quantify this chance for escape, one calculates the singlet-to-triplet yield $\Phi_{ST}$.

To find the triplet yield it is useful to consider the following diagram:

$$\begin{array}{ccc} S & \rightleftharpoons & T \\ \Big\downarrow{\scriptstyle k_S} & & \Big\downarrow{\scriptstyle k_T} \end{array} \qquad (1)$$

where $S(t)$ and $T(t)$ represent singlet and triplet state populations, respectively, and $k_S$ and $k_T$ give the rates at which these states depopulate. Note that there are typically two ways these states can depopulate: recombination at rate $k_R$ or escape from the cage at rate $k_E$. The latter is determined by diffusion and is likely independent of spin state. The former can depend on spin state and is typically such that the recombination of $S(t)$ or $T(t)$ dominates. Thus, for example, $k_S \simeq k_R + k_E$ while $k_T \simeq k_E$ and so $k_S \neq k_T$. Thus, in real systems, whatever effects $k_S$ and $k_T$ have on the steady field and frequency dependences of the singlet-to-triplet yield can be controlled by altering the diffusion rate, and this can be done by varying the solution viscosity, temperature, etc. Also note that in the equations that follow, $k_S$ and $k_T$ should have the same units as angular frequencies. Thus their units are given in radians per second.

Returning to diagram (1), if one starts with the initial condition $S(0) + T(0) = 1$ ($S(0) = 1$ for initial singlet state), $S(t)$ and $T(t)$ will decay with time until both equal zero. The triplet yield is defined as the fraction of radical pairs which depopulate from the triplet state (at the rate $k_T$) while the singlet yield is defined as the fraction which depopulate from the singlet state (at the rate $k_S$). Thus one has

$$\frac{d}{dt}\Phi_{ST}(t) = k_T T(t) \tag{2}$$

or

$$\Phi_{ST}(t) = \int_0^t k_T T(t')\, dt'. \tag{3}$$

In the Schrödinger equation method [18], $k_S = k_T = 1/\tau$, and, if the initial state is singlet, one has $T(t) = e^{-t/\tau}\psi^*(t)Q_T\psi(t)$, where $\psi(t)$ is the wave function determined by

$$\frac{d}{dt}\psi(t) = -\frac{i}{\hbar}H(t)\psi(t)$$

and $Q_S$ and $Q_T$ are the singlet and triplet projection operators, respectively, that satisfy [18]

$$Q_S + Q_T = I, \tag{4}$$

where $I$ is the identity matrix, and

$$Q_T = \tfrac{3}{4} + S_1 \cdot S_2. \tag{5}$$

Meanwhile, in the Liouville formalism where $k_S$ and $k_T$ can be different, one must use $\rho(t)$, the density matrix representing the electron and nuclear spins at time $t$. In this formalism, the singlet and triplet populations at time $t$ are $S(t) = \mathrm{tr}[Q_S\rho(t)]$ and $T(t) = \mathrm{tr}[Q_T\rho(t)]$, respectively, where

$$\mathrm{tr}\, A = \sum_i A_{ii} \tag{6}$$

is the trace (sum of the diagonal elements) of the matrix $A$.

To determine $\rho(t)$ one specifies an initial condition such as $\rho(0) = Q_S/\mathrm{tr}\, Q_S$ for singlet, $\rho(0) = Q_T/\mathrm{tr}\, Q_T$ for triplet, or $\rho(0) = I/\mathrm{tr}\, I$ for diffusion randomized and integrates over time the Liouville equation [16]:

$$\frac{d\rho(t)}{dt} = -\frac{i}{\hbar}[H(t), \rho(t)]_- - \tfrac{1}{2}k_S[Q_S, \rho(t)]_+ - \tfrac{1}{2}k_T[Q_T, \rho(t)]_+, \tag{7}$$

where

$$[A, X]_\pm = AX \pm XA. \tag{8}$$

Note that the last two terms in Eq. (7) involve anti-commutators rather than products like $Q_S\rho(t)Q_S$ or $Q_T\rho(t)Q_T$. Haberkorn [22] shows why the form used here gives more reasonable results. Also note that the Hamiltonian $H(t)$ is typically a sum of Zeeman, hyperfine, and exchange interaction terms (all often assumed isotropic, as given here):

$$H(t) = g\mu_B \sum_{j=1}^{2}\left[B(t)\cdot S_j + a_j I_j \cdot S_j\right] + hJS_1 \cdot S_2. \tag{9}$$

Even though other terms can contribute, this Hamiltonian is sufficient for the systems discussed in this paper. Note that the methods discussed in this paper also apply for more general Hamiltonians, the most restricted being the rotating frame method which can only handle $g$, hyperfine, and exchange tensors that are axial or isotropic when a single rotating magnetic field is applied. Also note that in Eq. (9) $B(t)$ and $a_j$ are given in gauss while $J$ is given in MHz. The conversion factor $g\mu_B/h$ for $g = 2$ (as here) is 2.799222 MHz/G [23].

To determine the singlet or triplet yields, one must integrate $k_S S(t)$ or $k_T T(t)$ over time. Typically one wants to find $\Phi_{ST}(\infty)$ (often written as $\Phi_{ST}$), the steady-state singlet-to-triplet yield. This quantity is

$$\Phi_{ST}(\infty) = \int_0^\infty k_T T(t)\, dt = \int_0^\infty k_T\, \mathrm{tr}[Q_T\rho(t)]\, dt = k_T\, \mathrm{tr}[Q_T\hat{\rho}], \tag{10}$$

where

$$\hat{\rho} = \int_0^\infty \rho(t)\, dt. \tag{11}$$

Similarly, the steady state singlet-to-singlet yield is

$$\Phi_{SS}(\infty) = \int_0^\infty k_S S(t)\, dt = \int_0^\infty k_S\, \mathrm{tr}[Q_S\rho(t)]\, dt = k_S\, \mathrm{tr}[Q_S\hat{\rho}]. \tag{12}$$

Note that in the Liouville formalism the density matrix includes all nuclear spin states. Thus, unlike in the Schrödinger approach, one does not need to average over nuclear spin states.

For a time-independent Hamiltonian $H$, one can solve for singlet or triplet yields by integrating Eq. (7) over time. This gives, since $\rho(t)$ should always decay to zero with time, an equation for $\hat{\rho}$ (defined in Eq. (11)):

$$-\rho(0) = -\frac{\mathrm{i}}{\hbar}[H, \hat{\rho}]_- - \tfrac{1}{2}k_S[Q_S, \hat{\rho}]_+ - \tfrac{1}{2}k_T[Q_T, \hat{\rho}]_+, \quad (13)$$

which is a matrix equation of the form

$$A\hat{\rho} + \hat{\rho}B = C, \quad (14)$$

where $A$, $B$, $C$, $H$, $\hat{\rho}$, $\rho(0)$, $Q_S$, and $Q_T$ are all $N \times N$ matrices. Equations of this type can be solved for $\hat{\rho}$ using the methods described in Refs. [24,25] or the useful algorithm given in Ref. [26]. Nevertheless, for time-dependent Hamiltonians $H(t)$, like those including oscillating fields, solving Eq. (13) is insufficient. Alternative methods are discussed below.

## 3. Typical treatments of oscillating fields

### 3.1. Numerical integration

A most general way to determine $\Phi_{ST}$ for time-dependent fields, $B(t)$, is to integrate the Liouville equation (7) using, for example, a 4th order Runge–Kutta scheme (a numerical method for solving ordinary differential equations [27, ch. 16]). This method can handle any time-dependent field and more general (e.g., less isotropic) Hamiltonians than in Eq. (9), but, since it involves numerical integration, its accuracy depends on the time step $\delta t$ and the number of steps $N_t$ used. That is, if $\delta t$ is too large, $\rho(t)$ will deviate significantly from its true path, causing increasing inaccuracies as the number of time steps increases. Thus, this method usually requires a large number of very small time steps, and, hence, tends to be quite computationally intensive and slow. It also gives very little insight into how the singlet-to-triplet yield varies with magnetic field strength or frequency. Thus, a better method is desired.

### 3.2. Rotating frame treatment

If the oscillating field is of the form

$$B(t) = B_0\hat{z} + B_1(\hat{x}\cos\omega t + \hat{y}\sin\omega t), \quad (15)$$

where $\hat{x}$, $\hat{y}$, $\hat{z}$ are mutually perpendicular unit vectors in a right-handed basis, the resulting time-dependent Hamiltonian $H(t)$ can be transformed from the laboratory frame into a reference frame rotating with the field $B_1(t)$ where it becomes a time-independent Hamiltonian $H'$. For example, if the laboratory frame Hamiltonian is as in Eq. (9), then the rotating frame Hamiltonian is [18]

$$H' = g\mu_B \sum_{j=1}^{2} (B_0 S_{jz} + B_1 S_{jx} + a_j I_j \cdot S_j) + hJS_1 \cdot S_2 - \hbar\omega \sum_{j=1}^{2} (S_{jz} + I_{jz}). \quad (16)$$

Note that the field $B(t)$ has been replaced by its steady component $B_0$ along $\hat{z}$ and its rotating component $B_1$ along the rotating frame's unit vector $\hat{x}$. Also note that a final term proportional to $\hbar\omega$ has been added to $H(t)$ to obtain $H'$. This final term includes the electron spin operators for the electrons that are involved in the Zeeman interaction with the rotating field $B_1(t)$ as well as the nuclear spin operators for the nuclei that couple to these electrons. Finally note that if the Zeeman term due to the steady field $B_0$ is large compared to the hyperfine and exchange terms (as in RYDMR experiments [14, p. 115]), the $I_{jz}$ operators in the final term of $H'$ can be neglected. Nevertheless, for very weak steady fields $B_0$, it is important not to neglect these $I_{jz}$ terms [18].

One important advantage of the rotating frame treatment is that it allows the time-dependent Hamiltonian $H(t)$ to be transformed into a time-independent Hamiltonian $H'$, which allows quick and simple solution of its singlet-to-triplet yields. This method is, however, limited to the case in which the only time-dependent field is rotating, the steady field is either negligible or along the axis of rotation of the rotating field, and the matrices of the Zeeman, hyperfine, and exchange terms are either isotropic or axially symmetric about the axis of the steady field. Thus, if one hopes to deal with more general field configurations, the interaction of multiple frequencies of oscillating field, or anisotropic Zeeman, hyperfine, or exchange interactions, this method will not suffice.

## 4. Perturbation theory treatment

### 4.1. Derivation

The first step in the perturbation theory treatment is to write the external magnetic field as

$$B(t) = B_0 + \lambda B_1(t) = B_0 + \sum_{j=1}^{N_E} \lambda B1\, j\, e^{i\alpha_j t}, \quad (17)$$

where $N_E$ is twice the number $N_p$ of oscillating fields applied and $\lambda$ is the perturbation parameter which later gets set equal to one. Such an expansion can always be done for periodic $B_1(t)$'s. From this one obtains a time-dependent Hamiltonian $H(t)$ made up of a time-independent $H_0$ and a time-dependent perturbation $V(t)$:

$$H(t) = H_0 + \lambda V(t) = H_0 + \sum_{j=1}^{N_E} \lambda V_j\, e^{i\alpha_j t}. \quad (18)$$

Then, as usual when applying perturbation theory, one must assume that $B_1(t)$ and all its time-independent $B_{1j}$ vectors are much smaller than $B_0$ in magnitude and that $V(t)$ and all its time-independent $V_j$ matrices are much smaller than $H_0$ (or, equivalently, that the perturbations are applied for a very short time).

Next, using

$$D_j = -\frac{i}{\hbar} V_j,$$

$$E = -\frac{i}{\hbar} H_0 - \tfrac{1}{2}(k_S Q_S + k_T Q_T),$$

and

$$F = \frac{i}{\hbar} H_0 - \tfrac{1}{2}(k_S Q_S + k_T Q_T),$$

one obtains from Eqs. (7) and (18)

$$\frac{d\rho(t)}{dt} = E\rho(t) + \rho(t)F + \sum_{j=1}^{N_E} e^{i\alpha_j t}\lambda\left[D_j, \rho(t)\right]_-. \quad (19)$$

Then, putting

$$\rho(t) = \sum_{l=0}^{\infty} \rho_l(t)\lambda^l \quad (20)$$

into Eq. (19), one can equate powers of $\lambda$ to obtain for $l = 0$

$$\frac{d\rho_0(t)}{dt} = E\rho_0(t) + \rho_0(t)F, \quad (21)$$

and for $l \geq 1$

$$\frac{d\rho_l(t)}{dt} = E\rho_l(t) + \rho_l(t)F + \sum_{j=1}^{N_E} e^{i\alpha_j t}\left[D_j, \rho_{l-1}(t)\right]_-. \quad (22)$$

Next, it is convenient to set $\rho_0(0) = \rho(0)$ and $\rho_l(0) = 0$ for $l \geq 1$. Also, since for $k_S, k_T > 0$ the density matrix decays to zero with time, one sets $\rho_l(\infty) = 0$ for $l \geq 0$. Then, if one defines

$$P_l(\alpha) = \int_0^{\infty} \rho_l(t)\, e^{i\alpha t}\, dt, \quad (23)$$

integrating by parts yields

$$P_l(\alpha) = \frac{1}{i\alpha}\left( \rho_l(t)\, e^{i\alpha t}\Big|_0^{\infty} - \int_0^{\infty} \frac{d\rho_l(t)}{dt}\, e^{i\alpha t}\, dt \right). \quad (24)$$

Then, inserting Eqs. (21) and (22) gives for $l = 0$

$$P_0(\alpha) = \frac{i}{\alpha}\left( \rho(0) + \int_0^{\infty} \left[E\rho_0(t) + \rho_0(t)F\right] e^{i\alpha t}\, dt \right) = \frac{i}{\alpha}\left[ \rho(0) + EP_0(\alpha) + P_0(\alpha)F \right], \quad (25)$$

while for $l \geq 1$ it gives

$$P_l(\alpha) = \frac{i}{\alpha}\left[ \int_0^{\infty} \left( E\rho_l(t) + \rho_l(t)F + \sum_{j=1}^{N_E} e^{i\alpha_j t}\left[D_j, \rho_{l-1}(t)\right]_- \right) e^{i\alpha t}\, dt \right] = \frac{i}{\alpha}\left( EP_l(\alpha) + P_l(\alpha)F + \sum_{j=1}^{N_E} \left[D_j, P_{l-1}(\alpha + \alpha_j)\right]_- \right). \quad (26)$$

These equations then give a series that can be iterated to obtain any $P_l(\alpha)$.

Next, since

$$\hat{\rho}_l = \int_0^\infty \rho_l(t)\, \mathrm{d}t = P_l(0), \tag{27}$$

one obtains from Eqs. (21) and (22) or from Eqs. (25) and (26) that for $l = 0$

$$-\rho(0) = E\hat{\rho}_0 + \hat{\rho}_0 F, \tag{28}$$

and for $l \geqslant 1$

$$0 = E\hat{\rho}_l + \hat{\rho}_l F + \sum_{j=1}^{N_E} \left[ D_j,\, P_{l-1}(\alpha_j) \right]_-. \tag{29}$$

### 4.2. Summary of results

Thus, in summary, to obtain $\Phi_{ST}$ one simply sets $\lambda = 1$ and uses

$$\Phi_{ST} = k_T\, \mathrm{tr}[Q_T \hat{\rho}] = k_T\, \mathrm{tr}\left[ Q_T \sum_{l=0}^{l_{max}} \hat{\rho}_l \right]$$

$$= \sum_{l=0}^{l_{max}} k_T\, \mathrm{tr}[Q_T \hat{\rho}_l] = \sum_{l=0}^{l_{max}} \Phi_{ST}^{(l)}, \tag{30}$$

where $l_{max}$ is the maximum order of perturbation theory to be used and where $\hat{\rho}_0$ satisfies

$$-\rho(0) = E\hat{\rho}_0 + \hat{\rho}_0 F \tag{31}$$

and $\hat{\rho}_l$ for $l \geqslant 1$ satisfy

$$0 = E\hat{\rho}_l + \hat{\rho}_l F + \sum_{j=1}^{N_E} \left[ D_j,\, P_{l-1}(\alpha_j) \right]_-. \tag{32}$$

Of course, one must also use the results for $l = 0$

$$P_0(\alpha) = \frac{\mathrm{i}}{\alpha} \left[ EP_0(\alpha) + P_0(\alpha) F + \rho(0) \right], \tag{33}$$

and for $l \geqslant 1$

$$P_l(\alpha) = \frac{\mathrm{i}}{\alpha} \left( EP_l(\alpha) + P_l(\alpha) F + \sum_{j=1}^{N_E} \left[ D_j,\, P_{l-1}(\alpha + \alpha_j) \right]_- \right). \tag{34}$$

### 4.3. Implementation details

These last two equations both have the form

$$X = \frac{\mathrm{i}}{\alpha} [EX + XF - C], \tag{35}$$

or equivalently

$$C = [E + \mathrm{i}\alpha/2]X + X[F + \mathrm{i}\alpha/2], \tag{36}$$

which is of the form

$$AX + XB = C. \tag{37}$$

Eqs. (31) and (32) (the other main equations used in this method) are also of this form. This type of equation can easily be solved for the complex matrices $A$, $B$, $C$, and $X$ used here with the algorithm given in Ref. [26] and a useful trick [27, pp. 50, 481, 482] that works for any group of complex matrices in the equations used here. The trick is to set, for example,

$$\tilde{A} = \begin{pmatrix} \mathrm{Re}\, A & -\mathrm{Im}\, A \\ \mathrm{Im}\, A & \mathrm{Re}\, A \end{pmatrix} \tag{38}$$

so that $\tilde{A}$, $\tilde{B}$, $\tilde{C}$, and $\tilde{X}$ are $2N \times 2N$ real matrices based on the $N \times N$ complex matrices $A$, $B$, $C$, and $X$. The algorithm can then be used to solve $\tilde{A}\tilde{X} + \tilde{X}\tilde{B} = \tilde{C}$ for the real matrix $\tilde{X}$, and then the complex matrix $X$ can be found from the elements of $\tilde{X}$.

Ideally, however, one would like to solve $AX + XB = C$ directly for complex matrices, but Ref. [27, pp. 50, 482] says that for similar problems solving the complex $N \times N$ case directly is in principle only two times faster than solving the real $2N \times 2N$ case.

A number of methods for solving $AX + XB = C$ have been discussed over the years [24,25], and it may be that some of these give better-performing algorithms than the one used here. For example, one paper [24] discusses a method that should run 30% faster than the one used here, but no source code is given.

Finally, the breaking up of $\alpha$ in Eq. (36) is rather arbitrary. It may be that other equivalent expressions such as the one with $A = E + \mathrm{i}\alpha$ and $B = F$ work better, perhaps being solved faster or more reliably than the expression used here.

### 4.4. Execution times

Examining the heart of the Liouville perturbation method (Eqs. (30)–(34)), one can see that many

$AX + XB = C$ equations must be solved. For example, for $l_{max} = 0$ there is only one such equation to solve, but for $l_{max} = 1$ there are $1 + 1 + N_E$. In fact, for a given $m = l_{max}$ there are $\mathrm{tot}_m$ such equations to solve, each typically scaling as $N^3$, where $\mathrm{tot}_m$ is

$$\begin{aligned}\mathrm{tot}_m &= 1 + (1 + N_E) + (1 + N_E + N_E^2) + \ldots \\ &\quad + (1 + N_E + N_E^2 + \ldots + N_E^m) \\ &= (m+1) + (m+0)N_E + (m-1)N_E^2 \\ &\quad + (m-2)N_E^3 + \ldots + (1)N_E^m \\ &= \sum_{r=0}^{m} N_E^r (m+1-r) = \sum_{r=0}^{m} N_E^{m-r}(r+1).\end{aligned} \tag{39}$$

For $N_E = 2$, the first few values of $\mathrm{tot}_m$ are 1, 4, 11, 26, 57, 120, and 247, whereas for $N_E = 4$, the first few values are 1, 6, 27, 112, 453, 1818, and 7279 for $m = 0$, 1, 2, 3, 4, 5, and 6, respectively. Notice how for large $m$, $\mathrm{tot}_{m+1}$ approaches $N_E \mathrm{tot}_m$. This is because

$$\begin{aligned}\mathrm{tot}_{m+1} &= \sum_{r=0}^{m+1} N_E^{m+1-r}(r+1) \\ &= N_E \sum_{r=0}^{m} N_E^{m-r}(r+1) + (m+2) \\ &= N_E \mathrm{tot}_m + m + 2.\end{aligned} \tag{40}$$

Thus it is good to keep $N_E$ to a minimum.

The minimum number of perturbing Hamiltonians $N_E$ needed for an oscillating field is two. Thus, if there are multiple perturbations at the same frequency, it is good to pool them into one $e^{i\alpha_j t}$ and one $e^{-i\alpha_j t}$ term. Although sometimes phase and orientation relations among the different oscillating perturbing fields can complicate this pooling, the savings in computer time, especially for high $l_{max}$, makes it well worth the effort.

Table 1 lists typical execution times in CPU seconds on an IBM RS6000/320H workstation for the Runge–Kutta, rotating frame, and perturbation methods in the Liouville formalism (described in this paper) and in the Schrödinger formalism (described in a previous paper [18]). Notice how the perturbation method is much faster for large $l_{max}$ in the Liouville than in the Schrödinger formalism. Also notice the rough agreement of the times in Table 1 with the predicted scaling rules ($N^3$ for the Liouville Runge–Kutta, rotating frame, and perturbation methods) as well as the predicted rise in perturbation method execution time with $l_{max}$ (1, 11, 57, 247, 1013, 4083, and 16369 for $l_{max} = 0$, 2, 4, 6, 8, 10, and 12, respectively when $N$ is fixed and $N_E = 2$).

Although both scale as $N^3 N_t$, one reason that the Liouville Runge–Kutta method goes slower than the Schrödinger Runge–Kutta method may be that the Liouville equation uses an $N \times N$ density matrix $\rho(t)$ while the Schrödinger equation uses for initial singlet states $N_S = N/4$ different wave functions

Table 1
Typical times spent on an IBM RS6000/320H workstation calculating points as in Figs. 1 and 2 but with $I_1 = 1/2$, 3/2, or 7/2 ($N = 8$, 16, or 32) and $N_E = 2$ (Liouville formalism) or $N_p = 1$ (Schrödinger formalism). Times are given for methods based on the Liouville equation (described in this paper) and the Schrödinger equation (see Ref. [18])

| Method | Liouville formalism | | | | Schrödinger formalism | | | |
|---|---|---|---|---|---|---|---|---|
| | time (CPU sec) | | | effective scaling | time (CPU sec) | | | effective scaling |
| | $N = 8$ | $N = 16$ | $N = 32$ | | $N = 8$ | $N = 16$ | $N = 32$ | |
| Runge–Kutta ($N_t = 5000$) | 163.68 | 446.40 | 1863.17 | $N^{1-3}$ | 222.00 | 436.69 | 958.22 | $N^{0-2}$ |
| rotating frame | 0.12 | 0.34 | 1.61 | $N^{1-3}$ | 0.12 | 0.16 | 0.48 | $N^{0-2}$ |
| perturbation ($l_{max} = 2$) | 0.49 | 2.24 | 14.61 | $N^{2-3}$ | 4.10 | 29.12 | 183.89 | $N^{2-3}$ |
| perturbation ($l_{max} = 4$) | 2.15 | 11.17 | 76.10 | $N^{2-3}$ | 210.44 | 3885.10 | 13525.01 | $N^{1-5}$ |
| perturbation ($l_{max} = 6$) | 9.12 | 47.76 | 331.63 | $N^{2-3}$ | | | | |
| perturbation ($l_{max} = 8$) | 35.50 | 189.99 | 1339.93 | $N^{2-3}$ | | | | |
| perturbation ($l_{max} = 10$) | 142.07 | 766.21 | 5423.57 | $N^{2-3}$ | | | | |
| perturbation ($l_{max} = 12$) | 569.88 | 3070.71 | 21719.51 | $N^{2-3}$ | | | | |

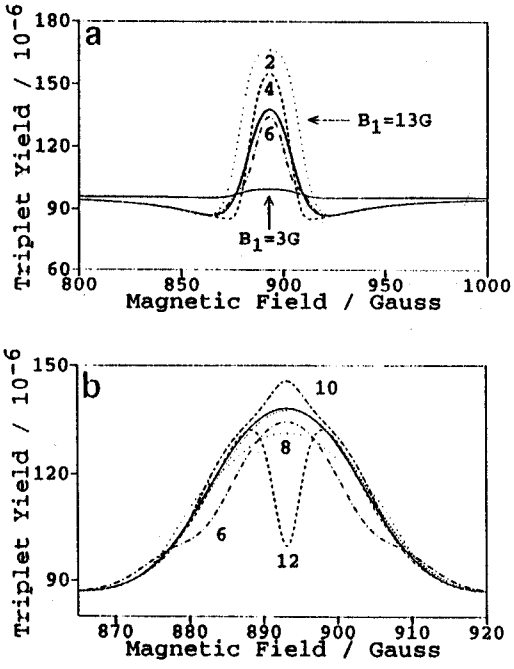


Fig. 1. Comparison of singlet-to-triplet yields calculated using Runge–Kutta (finely dotted lines), rotating frame (solid lines), and perturbation methods in the Liouville formalism. Here $g = 2$, $B_1(t)$ is a field rotating counterclockwise about $B_0$ at frequency 2.5 GHz, only one nuclear spin with $I_1 = 1/2$ and $a_1 = 0.5$ G is included, $J = 39.1891$ MHz (14 G), and $\tau = 5$ ns. Runge–Kutta points use $N_t = 5000$ and $\delta t = 0.03$ ns. In both plots $B_0$ is varied but orders of perturbation theory $l_{max}$ and $B_1$ used differ in each. Curves for odd $l_{max}$ coincide with curves for $l_{max} - 1$. (a) $B_1 = 3$ or 13 G and $l_{max} = 2$ (sparsely dotted), 4 (dashed), or 6 (dot-dashed). The curves for $B_1 = 3$ G are practically coincident and so are not labelled individually. (b) $B_1 = 13$ G and $l_{max} = 6$ (dot-dashed), 8 (sparsely dotted), 10 (dash-dashed), or 12 (dashed).

$\psi(t)$, each of which is an expansion in terms of $N$ different eigenvectors (for initial triplet states it uses $3N_S = 3N/4$ different wave functions $\psi(t)$). This may also explain why the Liouville rotating frame method is slower than the Schrödinger rotating frame method. It may also be that solving $AX + XB = C$ takes longer than diagonalizing Hamiltonians, even though both scale as $N^3$ [26; 27, ch. 11]. If this were so, it could account for the different execution times in the rotating frame methods.

Finally, comparing Table 1 with Tables 1 and 2 in Ref. [18] shows slight changes in the speed of the Schrödinger equation methods. These differences are due to minor algorithm changes and improved use of certain compiler options on the RS6000 after Ref. [18] was written.

## 5. Comparison of methods

Figs. 1–3 all give results for Hamiltonian (9) when $g = 2$, $S_1 = S_2 = I_1 = 1/2$, $I_2 = 0$, $a_1 = 0.5$ G, $a_2 = 0$ G, and $J = 39.1891$ MHz (14 G) for Figs. 1 and 2 or $J = 0$ MHz for Fig. 3. The parameters for Figs. 1 and 2 were chosen to give results as in Fig. 1 of Ref. [15] while those for Fig. 3 were chosen because they yield interesting effects. Incidentally, a number of real systems have $I_1 = 1/2$ nuclei with hyperfine constants $a_1$ near 0.5 G; for example, certain hydrogens in biphenyl anions and polyacenes have $a_1$ between 0.39 and 0.98 G [23, pp. 63, 65, 105] while Y@$C_{82}$ fullerene complexes have $a_1 =$ 0.48 G [28] and $O^-$ ions in natural zircon crystals interact with $^{89}Y$ nuclei having $a_1 = 0.34$ G [29]. Finally, a number of different $B_0$, $B_1(t)$, $\tau$, $k_S$, and $k_T$ values are used in Figs. 1–3 (see captions for details).

Figs. 1a, 2, 3b, and 3e repeat Figs. 4a, 4b, 5a, and 5b of Ref. [18], this time being calculated using the Liouville equation when $k_S = k_T = 1/\tau$. The results shown here are practically indistinguishable from the ones there except that in Figs. 1 and 2 the Liouville Runge–Kutta method agrees slightly better with the other methods than did the Schrödinger Runge–Kutta

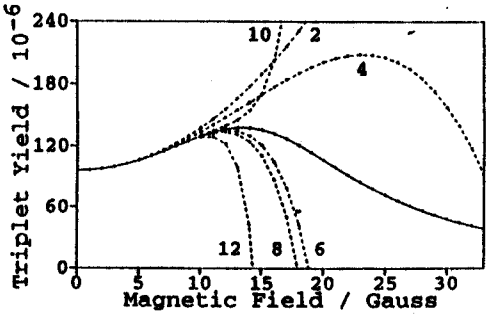


Fig. 2. Comparison of singlet-to-triplet yields calculated using Runge–Kutta (dotted lines), rotating frame (solid lines), and perturbation (dashed lines) methods in the Liouville formalism. Parameters same as in Fig. 1 except here $B_0$ is fixed at resonance (893.1053 G) and $B_1$ is varied from 0 to 33 G with 1 G increments. Perturbation orders $l_{max} = 2$, 4, 6, 8, 10, and 12 are used. Curves for odd $l_{max}$ coincide with curves for $l_{max} - 1$.

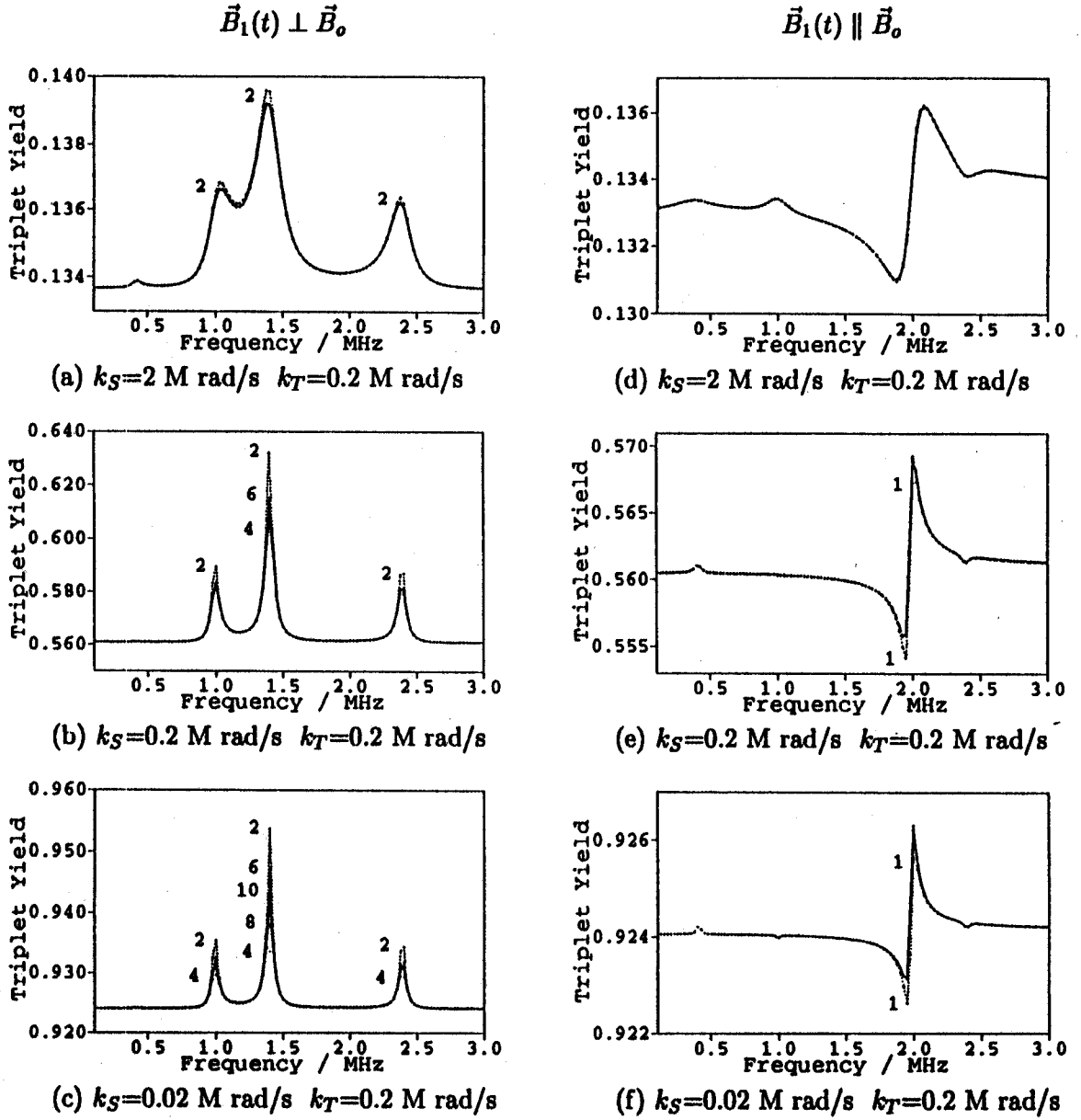


Fig. 3. Comparison of singlet-to-triplet yields calculated using Runge–Kutta (dashed lines), rotating frame (solid lines), and perturbation (dotted lines) methods in the Liouville formalism. Here, $g = 2$, $B_0 = 0.5$ G, $B_1(t)$ oscillates at frequencies from 0.1 to 3 MHz (0.025 MHz increments) and has $B_1 = 0.007$ G, only one nuclear spin with $I_1 = 1/2$ and $a_1 = 0.5$ G is included, and $J = 0$. Runge–Kutta points use $N_t = 10000$ and $\delta t = 15$ ns. $k_S$ and $k_T$ are also varied from plot to plot. In (a)–(c) $B_1(t)$ rotates counterclockwise about $B_0$ and $l_{max} = 2$, 4, 6, 8, or 10. Orders alternate being above and below Runge–Kutta and rotating frame results (2 up, 4 down, etc.). In (d)–(f) $B_1(t)$ is a linear oscillation along $B_0$ such that $B(0) = B_0 + B_1$ and $l_{max} = 1$, 2, 3, 4, 5, 6, 7, 8, 9, or 10. In (a)–(f) orders that clearly stand out from the rest are numbered. Rotating frame is only used in plots (a)–(c). Plots (b) and (e) repeat Figs. 5a and 5b in Ref. [18]. Plots come in pairs with same $k_S$, $k_T$ values: (a) and (d), (b) and (e), and (c) and (f).

method in Ref. [18]. Another difference is that in the same execution time the Liouville perturbation method can go to much higher $l_{max}$ than the Schrödinger perturbation method.

Figs. 1, 2, and 3 have a number of things in common. Most of them show good agreement among the different methods, especially for weak oscillating fields, and the Runge–Kutta and rotating frame methods typically give indistinguishable results. These figures also show that as $l_{max}$ rises, the perturbation method usually agrees better with the other methods. When this happens, the perturbation series is said to converge and typically only the first few orders are needed to approximate the overall effect well. Although general rules for convergence are beyond the scope of this paper (and perhaps more easily derived for the $k_S = k_T = 1/\tau$ case using the Schrödinger perturbation method in Ref. [18]), in practice one can determine convergence by comparing at points where $B_1(t)$ has a large effect (such as near $B_0 = 893$ G in Fig. 1) perturbation results from the first few orders $l_{max}$ and, if possible, doing spot checks against Runge–Kutta results. If the results are not convergent, one simply reduces $B_1$ until they converge.

Next, each plot shows that for rotating fields, only even orders contribute [18], while for parallel fields, odd orders can contribute (see Figs. 3e and 3f where $l_{max} = 1$ stands out from the rest). That only even orders contribute for rotating fields is best seen in Fig. 2 where the differences between the $l_{max}$ and $l_{max} - 2$ curves all go as $B_1^{l_{max}}$. As discussed in Ref. [18], this effect is due to the fact that for a rotating field the symmetry of the system prevents the sign of $B_1$ from affecting the overall yield. Thus odd orders of perturbation theory do not contribute for rotating fields.

Nevertheless, each of the figures has its own unique features. For example, Fig. 1 shows a range around the peak (near 893 G) in which the perturbation method does not converge with increasing $l_{max}$. However, this figure also shows that this range narrows as $l_{max}$ rises. Fig. 2 shows a similar effect, this time showing a cutoff with respect to $B_1$; that is, beyond a certain $B_1$ value (around 10 G here), higher $l_{max}$ values give worse results, the series diverges, and perturbation theory is said to break down. From the trend in Fig. 2, it seems that higher order terms approach $\pm\infty$ at the breakdown field value.

Next, Fig. 3 shows a number of things. It shows one system at several different $k_S$, $k_T$ values when rotating or parallel oscillating fields are used. First note the close agreement among all the different methods used, even when $k_S \neq k_T$. Next note that higher $\tau$ (lower $k_S$, $k_T$) gives a less convergent perturbation series (for example, compare 3a with 3c or compare 3d with 3e and 3f). This is less apparent in the parallel oscillation plots where by $l_{max} = 2$ the plots have converged considerably. Nevertheless, in the rotating oscillation plots, the series take several orders to converge, thus allowing one to see how different orders contribute. As in [18], only even orders contribute, and, for this particular system, the orders seem to alternate being above and below the results from the other methods ($l_{max} = 2$ is above, 4 is below, etc.).

Also note in Fig. 3 the effects of varying $k_S$, $k_T$ on singlet-to-triplet yields. One can see substantial changes in the baseline yields as well as variations in the peak heights and line widths of the frequency dependent parts of the yields. In fact, it is apparent that different peaks are affected in different ways by $k_S$, $k_T$ variations, allowing the relative importance of different frequencies to be altered by changing $k_S$, $k_T$. Such effects could, in principle, be measured by an experimenter by varying solution viscosity, temperature, etc. Such effects could also be exploited in biological systems allowing, for example, magnetic field receptors to work better in one cellular compartment than another. Although these effects are interesting and give an incentive for using this new Liouville perturbation method, a detailed discussion of them is beyond the scope of this paper.

Finally, using $l_{max} = 0$, the Liouville method described here has reproduced Figs. 4–6 of Ref. [16] (data not shown).

## 6. Conclusion

This paper has presented a perturbation method based on the Liouville equation for treating oscillating magnetic fields in the radical pair mechanism. This method is much faster and more reliable than a similar perturbation method based on the Schrö-

dinger equation [18]. This new method can also serve better as a base for more complicated, thorough, rigorous treatments including, for example, rotational correlations, spin relaxation, multi-state processes, and complex rate equations. The Liouville perturbation method is also more general and applicable than the rotating frame method, since it allows fully anisotropic $g$, hyperfine, and exchange tensors and can treat any combination of a steady field with one or more oscillating fields at different frequencies, phases, and orientations with respect to the steady field. It is also much faster than the Runge–Kutta method, especially in the limit of small $k_S$, $k_T$ where one must use a large number $N_t$ of Runge–Kutta time steps.

Since this perturbation method works best when oscillating fields are very weak compared to the steady field, it should be applicable to studies of magnetic sensory mechanisms in animals (which evolved in the natural magnetic environment where oscillating fields are much weaker than steady fields) as well as to studies of health effects of oscillating magnetic fields.

## Acknowledgement

This work was conducted at the University of Illinois in Urbana-Champaign in the Illinois Electron Paramagnetic Resonance Research Center (NIH Grant P41RR01811) and in the Resource for Concurrent Biological Computing (NIH Grant P41RR05969). Support was also provided by a Department of Defense National Defense Science and Engineering Graduate Fellowship, administered by the United States Air Force, and an NIH Traineeship in Radiation Oncology (NIH Grant PHS 5 T32 CA 09067) awarded to J.M. Canfield. Special thanks go to Dr. Michael Heath of the Department of Computer Science and the National Center for Supercomputing Applications for his help in locating the $AX + XB = C$ algorithm used in this paper and to Dr. R.B. Clarkson of the College of Veterinary Medicine for his support and advice.

## References

[1] J.B. Phillips and S.C. Borland, Nature 359 (1992) 142.
[2] W. Wiltschko, U. Munro, H. Ford and R. Wiltschko, Nature 364 (1993) 525.
[3] R.J. Reiter, Regul. Toxicol. Pharmacol. 15 (1992) 226.
[4] R.J. Reiter, J. Cellular Biochemistry 51 (1993) 394.
[5] K. Schulten, C.E. Swenberg and A. Weller, Z. Physik. Chem. NF111 (1978) 1.
[6] K. Schulten, in: Festkörperprobleme, Vol. 22, ed. J. Treusch (Vieweg, Braunschweig, 1982) p. 61.
[7] K. Schulten and A. Weller, Die Umschau 25/26 (1984) 779.
[8] K. Schulten, in: Biological effects of static and extremely low frequency magnetic fields, ed. J.H. Bernhard (MMV-Medizin Verlag, Munich, 1986) p. 133.
[9] K. Schulten and A. Windemuth, in: Springer proceedings in physics, Vol. 11. Biophysical effects of steady magnetic fields, eds. G. Maret, N. Boccara and J. Kiepenheuer (Springer, Berlin, 1986) p. 99.
[10] K. McLauchlan, Physics World 5 (Jan. 1992) 41.
[11] K. McLauchlan, Physics World 5 (Sep. 1992) 17.
[12] A.J. Hoff, H. Rademaker, R. van Grondelle and L.N.M. Duysens, Biochim. Biophys. Acta 460 (1977) 547.
[13] A.J. Hoff, Photochem. Photobiol. 43 (1986) 727.
[14] W. Lersch and M.E. Michel-Beyerle, Chem. Phys. 78 (1983) 115.
[15] W. Lersch and M.E. Michel-Beyerle, Chem. Phys. Letters 136 (1987) 346.
[16] H.-J. Werner, K. Schulten and A. Weller, Biochim. Biophys. Acta 502 (1978) 255.
[17] J.L. Gould, Ann. Rev. Physiol. 46 (1984) 585.
[18] J.M. Canfield, R.L. Belford, P.G. Debrunner and K.J. Schulten, Chem. Phys. 182 (1994) 1.
[19] K.M. Salikhov, Y.N. Molin, R.Z. Sagdeev and A.L. Buchachenko, Studies in physical and theoretical chemistry, Vol. 22. Spin polarization and magnetic effects in radical reactions, ed. Y.N. Molin (Elsevier, Budapest, 1984).
[20] U.E. Steiner and T. Ulrich, Chem. Rev. 89 (1989) 51.
[21] N.J. Turro, Proc. Natl. Acad. Sci. USA 80 (1983) 609.
[22] R. Haberkorn, Mol. Phys. 32 (1976) 1491.
[23] J.E. Wertz and J.R. Bolton, Electron spin resonance: elementary theory and practical applications (Chapman and Hall, New York, 1986).
[24] G.H. Golub, S. Nash and C.V. Loan, IEEE Trans. Automatic Control AC-24 (1979) 909.
[25] A. Jameson, SIAM J. Appl. Math. 16 (1968) 1020.
[26] R.H. Bartels and G.W. Stewart, Commun. ACM 15 (1972) 820.
[27] W.H. Press, S.A. Teukolsky, W.T. Vetterling and B.P. Flannery, Numerical recipes in C: the art of scientific computing, 2nd Ed. (Cambridge Univ. Press, New York, 1992).
[28] J.H. Weaver et al., Chem. Phys. Letters 190 (1992) 460.
[29] V.M. Vinokurov et al., Soviet Phys. Cryst. 16 (1971) 262.